Potential of Constraining the Fifth Force Using the Earth as a Spin and Mass Source from Space

Zheng-Ting Lai(赖政廷)[1], Jun-Xu Lu(陆俊旭)[1*], Li-Sheng Geng(耿立升)[2,1,3,4,5*], Kai Wei(魏凯)[6], and Wei Ji(季伟)[7,8]

[1]*School of Physics, Beihang University, Beijing 102206, China*
[2]*Sino-French Carbon Neutrality Research Center, École Centrale de Pékin/School of General Engineering, Beihang University, Beijing 100191, China*
[3]*Peng Huanwu Collaborative Center for Research and Education, Beihang University, Beijing 100191, China*
[4]*Beijing Key Laboratory of Advanced Nuclear Materials and Physics, Beihang University, Beijing 102206, China*
[5]*Southern Center for Nuclear Science Theory (SCNT), Institute of Modern Physics, Chinese Academy of Sciences, Huizhou 516000, China*
[6]*School of Instrumentation Science and Opto-electronics Engineering, Beihang University, Beijing 100191, China*
[7]*Johannes Gutenberg University, Mainz 55128, Germany*
[8]*Helmholtz Institute Mainz, Mainz 55128, Germany*

(Received 4 October 2025; accepted manuscript online 9 February 2026)

We explore the potential of conducting an experiment in a low Earth orbit spacecraft and using the Earth as a spin and mass source to constrain beyond-the-standard-model (BSM) long-range spin- and velocity-dependent interactions, which are mediated by the exchange of an ultralight ($m_{Z'} < 10^{-10}$ eV) or massless intermediate vector boson. The high speed of low-Earth-orbit spacecraft can enhance their sensitivity to velocity-dependent interactions. This periodicity enables efficient signal extraction from background noise, thereby improving the accuracy of the experiment. Combining these advantages, we theoretically demonstrate that the novel spacecraft-Earth model can improve the existing bounds on these exotic interactions by up to three orders of magnitude using the China Space Station (CSS) as a representative low-Earth-orbit carrier. If successfully implemented, this model may provide an innovative strategy for detecting ultralight dark matter and yield tighter constraints on certain coupling constants of exotic interactions.

DOI: 10.1088/0256-307X/43/3/030202 CSTR: 32039.14.0256-307X.43.3.030202

Introduction. The Standard Model (SM) of particle physics has proven to be the most successful theory for describing the fundamental building blocks of nature and their interactions, and has been extensively tested across multiple fields of physics. However, new physics beyond SM have been eagerly sought to explain unresolved phenomena, such as dark matter,[1] dark energy,[2] strong CP violation,[3] the matter-antimatter asymmetry,[4] and the hierarchy problem.[5] Among the numerous attempts to extend the SM, the idea of an additional fundamental interaction beyond the well-known strong, weak, electromagnetic, and gravitational forces has emerged as one of the most promising solutions. This hypothetical interaction is often referred to as a fifth force.[6,7]

Hypothetical fifth forces can generally be classified into two categories: those that depend on the spins[8–10] and those that do not.[11] The former, also known as exotic spin-dependent interactions, can be interpreted as a new type of long-range force mediated between fermions via novel light or massless particles, including spin-0 axion-like particles (ALPs),[3,12,13] spin-1 bosons,[9] dark photons,[14,15] and pairs of fermions,[16–18] all of which are leading candidates for dark matter or dark energy.

Moody and Wilczek first proposed a formalism for the exotic spin-dependent interactions associated with an axion.[8] Later, it was shown that any interaction mediated by scalar and vector bosons could be expressed in 16 terms, each characterized by the spin, mass, distance, and relative velocity.[9] These potentials were recently revisited,[7,10] where they were categorized according to the type of physical coupling instead of the spin-momentum structure.[9] Meanwhile, various experiments have been proposed or performed to search for them, such as torsion balance or pendulum experiments,[19–23] torsional oscillator experiments,[24] spectroscopy,[25,26] comagnetometers,[27–32] trapped ions,[33] nitrogen-vacancy center in diamond,[34,35] neutron or polarized ^{3}He atoms[36] or other macroscopic experiments.[37–39] These experiments typically use a large collection of particles as a polarized spin source or an unpolarized mass source, along with sensitive spin sensors used to detect the resulting shifts in spin energy levels.

Depending on the size of the spin source, these experiments can be approximately divided into two categories: those using laboratory sources and those using the Earth,[31,37–41] Moon or Sun,[42–44] or asteroids[45] as an enormous source. Heckel *et al.* used unpolarized matter from the Earth or Sun to search for exotic velocity-dependent potentials between polarized electrons and unpolarized matter from the Sun and Moon.[42] Later, Hunter *et al.* utilized the Earth as a polarized electron source to investigate exotic spin- and velocity-dependent interactions.[38,39] Despite additional losses due to the distance between the polarized electrons and nucleons and the sensor, the enormous geoelectron and nucleon sources significantly improved the sensitivity for detecting exotic spin- and velocity-dependent interactions.[37–39] Relevant studies include experiments conducted by researchers at the National Institute of Standards and Technology,[46] University of Washington,[40] Amherst College,[37–39,47] Tsinghua University,[48] and California State University.[41] Note that the USTC team proposed a similar idea several days after our paper was posted on ArXiv.[49]

Compared to laboratory detection, the main drawbacks of using the Earth as a spin or mass source are the inability to

*Corresponding authors. Email: ljxwohool@buaa.edu.cn; lisheng.geng@buaa.edu.cn
© 2026 Chinese Physical Society and IOP Publishing Ltd. All rights, including for text and data mining, AI training, and similar technologies, are reserved.

directly modulate the source (although this can be achieved by rotating the experimental apparatus) and artificially controlling the location of the experiment, as well as the limited relative velocity resulting from Earth's rotation. Notably, these problems can be uniquely resolved by a low-Earth orbit spacecraft operating at altitudes of 100 to 2000 km, corresponding to an overall velocity of 6900–7900 m/s. Typical orbital altitudes for space stations such as the China Space Station (CSS) and International Space Station (ISS) are approximately 400 km. The corresponding nominal orbital velocity is approximately 7.67 km/s, which is more than 20 times that of the ground-based experiments.[38,39,42]

In addition, the orbit of a low-Earth orbital vehicle generally covers most of the Earth's surface. Assuming a typical low-Earth orbit, the vehicle orbits the Earth west to east with an orbital period of approximately 90 min, and its orbital plane has an inclination of 42°–43° with respect to the Earth's equatorial plane. In this way, the CSS covers the Earth's surface between 42° north and south latitudes, allowing experiments to be conducted in diverse locations, which is a key advantage, as emphasized in Refs. [37,50]. Thus, over time, with a low-Earth orbit spacecraft circling the Earth and the Earth's rotation, one anticipates unique periodic signals in the geomagnetic field. Spatially, measurements can be performed at any position, enabling exploration of the most stringent constraints with the same sensitivity.

In the current study, we propose a theoretical "Spacecraft-Earth" model, i.e., conducting an experiment on a low Earth orbit spacecraft, and explore the extent to which the constraints on the coupling constants of the fifth force can be improved solely by virtue of this new model.

Framework. In this study, we focused on the velocity-dependent interactions. To demonstrate the advantages of a space-based experiment better, we used the same framework employed by Hunter.[38] Following Ref. [51], the six exotic velocity-dependent spin–spin interactions are

$$\begin{aligned} V_{6,7} =& -\frac{\hbar}{8\pi c^2}\Big(\frac{g_{\rm V}^1 g_{\rm A}^2}{2M_1}+\frac{g_{\rm A}^1 g_{\rm V}^2}{2M_2}\Big) \\ &\times[(\hat{\boldsymbol{\sigma}}_1\cdot\boldsymbol{v})(\hat{\boldsymbol{\sigma}}_2\cdot\hat{\boldsymbol{r}})\pm(\hat{\boldsymbol{\sigma}}_1\cdot\hat{\boldsymbol{r}})(\hat{\boldsymbol{\sigma}}_2\cdot\boldsymbol{v})] \\ &\times\Big(1+\frac{r}{\lambda}\Big)\frac{{\rm e}^{-r/\lambda}}{r^2}, \end{aligned} \tag{1}$$

$$V_8 = \frac{g_{\rm A}^1 g_{\rm A}^2}{4\pi c^2}[(\hat{\boldsymbol{\sigma}}_1\cdot\boldsymbol{v})(\hat{\boldsymbol{\sigma}}_2\cdot\boldsymbol{v})]\frac{{\rm e}^{-r/\lambda}}{r}, \tag{2}$$

$$V_{14} = \frac{g_{\rm A}^1 g_{\rm A}^2}{4\pi c}[(\hat{\boldsymbol{\sigma}}_1\times\hat{\boldsymbol{\sigma}}_2)\cdot\boldsymbol{v}]\frac{{\rm e}^{-r/\lambda}}{r}, \tag{3}$$

$$\begin{aligned} V_{15} =& -\frac{g_{\rm V}^1 g_{\rm V}^2\hbar^2}{8\pi c^3 M_1 M_2} \\ &\times[(\hat{\boldsymbol{\sigma}}_1\cdot(\boldsymbol{v}\times\hat{\boldsymbol{r}}))(\hat{\boldsymbol{\sigma}}_2\cdot\hat{\boldsymbol{r}})+(\hat{\boldsymbol{\sigma}}_1\cdot\hat{\boldsymbol{r}})(\hat{\boldsymbol{\sigma}}_2\cdot(\boldsymbol{v}\times\hat{\boldsymbol{r}}))] \\ &\times\Big(3+\frac{3r}{\lambda}+\frac{r^2}{\lambda^2}\Big)\frac{{\rm e}^{-r/\lambda}}{r^3}, \end{aligned} \tag{4}$$

$$\begin{aligned} V_{16} =& -\frac{\hbar}{8\pi c^3}\Big(\frac{g_{\rm V}^1 g_{\rm A}^2}{2M_1}+\frac{g_{\rm A}^1 g_{\rm V}^2}{2M_2}\Big) \\ &\times[(\hat{\boldsymbol{\sigma}}_1\cdot(\boldsymbol{v}\times\hat{\boldsymbol{r}}))(\hat{\boldsymbol{\sigma}}_2\cdot\boldsymbol{v})+(\hat{\boldsymbol{\sigma}}_1\cdot\boldsymbol{v})(\hat{\boldsymbol{\sigma}}_2\cdot(\boldsymbol{v}\times\hat{\boldsymbol{r}}))] \\ &\times\Big(1+\frac{r}{\lambda}\Big)\frac{{\rm e}^{-r/\lambda}}{r^2}, \end{aligned} \tag{5}$$

where $g_{\rm V/A}$ denotes the vector (V) or axial (A) coupling constants of fermions 1 or 2 with spins $\hat{\boldsymbol{\sigma}}_{1/2}$ and masses $M_{1,2}$. The distance and relative speed between the two fermions are denoted by r and $\boldsymbol{v}$, $\hat{\boldsymbol{r}}$ are the unit vectors of the relative coordinates; $\lambda=\hbar/m'c$ is the reduced Compton wavelength of the boson of interest of mass m', representing the interaction range of the forces; $\hbar$ is the reduced Planck constant; and c is the speed of light in vacuum.

Although V_{4+5} could not provide the most stringent bounds as those of the lowest-order terms, it could probe different spin/velocity structures and confirm the types of couplings of the exchanged boson. Meanwhile, V_{12+13} takes the form of a Yukawa potential multiplied by the factor $\boldsymbol{\sigma}\cdot\boldsymbol{v}$, which may provide only access to couplings that might vanish in velocity-independent cases.[7] Similarly, a space-based experiment can shed light on these two interactions because of the significantly larger relative velocity, which reads[7,39,52]

$$V_{4+5}\big|_{\rm VV} = \frac{g_{\rm V}^{\rm e} g_{\rm V}^{\rm N}}{16\pi m_{\rm e}}\frac{\hbar^2}{c}\boldsymbol{\sigma}_{\rm e}\cdot(\boldsymbol{v}\times\hat{\boldsymbol{r}})\Big(\frac{1}{r^2}+\frac{1}{\lambda r}\Big){\rm e}^{-\frac{r}{\lambda}}, \tag{6}$$

$$V_{4+5}\big|_{\rm AA} = \frac{g_{\rm A}^{\rm e} g_{\rm A}^{\rm N}}{16\pi}\frac{\hbar^2}{c}\frac{m_{\rm e}}{m_{\rm N}^2}\boldsymbol{\sigma}_{\rm e}\cdot(\boldsymbol{v}\times\hat{\boldsymbol{r}})\Big(\frac{1}{r^2}+\frac{1}{\lambda r}\Big){\rm e}^{-\frac{r}{\lambda}}, \tag{7}$$

$$V_{12+13} = g_{\rm A}^1 g_{\rm V}^2\frac{\hbar}{4\pi}\boldsymbol{\sigma}_1\cdot\boldsymbol{v}\frac{{\rm e}^{-r/\lambda}}{r}. \tag{8}$$

Notably, velocity-independent interactions can constrain the coupling constants in Eqs. (1)–(8). For example, the $g_{\rm A}g_{\rm V}$ terms in $V_{6,7}$, V_{16}, and V_{12+13} can also be constrained by V_{11} (following the definition given in Ref. [7]. The most stringent limit on $g_{\rm A}g_{\rm V}$ for a characteristic length $\lambda > 9.9\times10^{-3}$ m was established by Heckel *et al.*[20] using the V_{11} term and for the range $10^3 < \lambda < 10^{11}$ m by Hunter *et al.*.[37] Similarly, the $g_{\rm A}g_{\rm A}$ term in $V_8, V_{14}, V_{4+5}|_{\rm AA}$ can also be constrained by V_2 and $V_3|_{\rm AA}$, and the $g_{\rm V}g_{\rm V}$ term in $V_{4+5}|_{\rm AA}$ and V_{15} is further constrained by $V_1, V_3|_{\rm VV}$. For the most stringent limits of these coupling constants from the velocity-independent interactions, refer to Ref. [7] for a detailed review. In most cases, velocity-independent interactions, that is, V_1, V_2, V_3, V_{11}, provide the most stringent limits for these couplings. However, velocity-dependent terms give rise to distinct types of interactions. This makes distinguishing between these interactions challenging.

The "Spacecraft-Earth" Model. We established a model of the Earth to describe the exotic velocity-dependent interactions between the Earth as the source and the spin sensor on a low-Earth-orbit spacecraft. The model involves its geoelectron density[37,53–55] and nucleon density,[39,53,56,57] which are denoted by $\rho_{\rm e}(r')$ and $\rho_{\rm n}(r')$, respectively, the internal temperatures $T(r')$, where r' represents the distance between the source particle and the center of the Earth, as well as the distribution of the geomagnetic field, $\boldsymbol{B}$, both inside and outside the Earth.

This model is based on Ref. [37], which assumes that Earth's paramagnetism is predominantly due to unpaired d-shell electrons in the iron ions contained within Earth's mantle and crust minerals. Using this assumption, the electron density was calculated. In this model, the density and temperature distributions are assumed to be spherically symmetric, and the Earth's core magnetization is neglected, as predicted by density functional theory calculations.[38] In addition, we adopt the temperature model in Ref. [58,59] and the updated World Magnetic Model (WMM 2020),[60,61] which is valid from 2020 to 2025 for Earth's magnetic field.

The planetary position and velocity of a low-Earth orbital spacecraft can be accurately obtained using the Skyfield package[62] with the corresponding TLE code.[63] In this study, we use $\boldsymbol{v}(r',\theta',\varphi',r'_{\rm s},\theta'_{\rm s},\varphi'_{\rm s})$ to represent the relative velocity between the spin sensor on the spacecraft and a specific geoelectron in Earth's mantle. Here, r', θ', φ', $r'_{\rm s}$, $\theta'_{\rm s}$, and $\varphi'_{\rm s}$ denote the spherical coordinates of the geoelectron and the spacecraft, respectively, with the center of the Earth as the origin, as shown in Fig. 1. The velocity resulting from Earth's rotation is given by $\boldsymbol{v}'=\boldsymbol{\Omega}\times\boldsymbol{r}'$. By combining this with $\boldsymbol{v}'_{\rm s}$, we can determine the relative velocity $\boldsymbol{v}=\boldsymbol{v}'_{\rm s}-\boldsymbol{v}'$, which is necessary for the calculations.

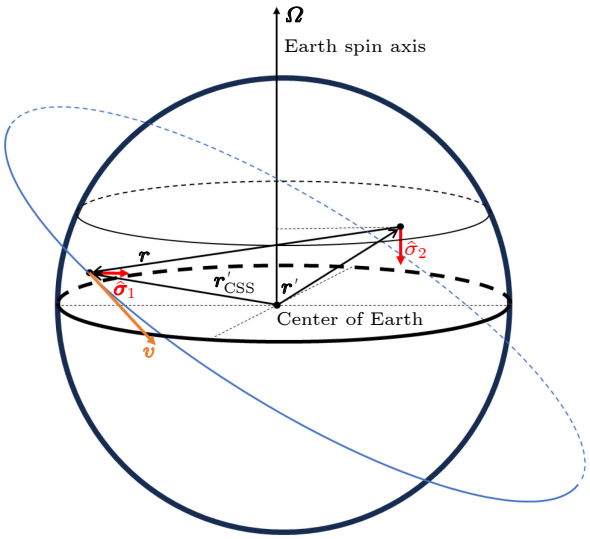

Fig. 1. Schematic layout of a space-based experiment. $\hat{\boldsymbol{\sigma}}_1$ represents the spin-sensitive direction of the apparatus on a low-Earth orbit spacecraft that is fixed geographically northward (N) or eastward (E). $\hat{\boldsymbol{\sigma}}_2$ represents the direction opposite the geomagnetic field. $\boldsymbol{r}'_{\rm s}$ and $\boldsymbol{r}'$ represent the radial positions of the spacecraft and geoelectron, respectively. $\boldsymbol{r}'_{\rm s} - \boldsymbol{r}'$ denote the relative position.

When summing the interactions between each polarized geoelectron inside the Earth and the spin sensor on the spacecraft, the total potential can be calculated as follows:

$$V_{\rm total} = \int_0^{2\pi}\int_0^{\pi}\int_{R_{\rm CM}}^{R_{\rm s}} r'^2 \sin\theta' \rho_{\rm e}(r') \frac{2\mu_{\rm B} B}{k_{\rm B} T(r')} \times V(\boldsymbol{r}, \boldsymbol{v}, r', \theta', \varphi', r'_{\rm s}, \theta'_{\rm s}, \varphi'_{\rm s}) {\rm d}r' {\rm d}\theta' {\rm d}\varphi', \quad (9)$$

where $\mu_{\rm B}$ is the Bohr magneton, $k_{\rm B}$ is Boltzmann's constant, and T is the temperature. The integration spanned the entire volume from the core-mantle boundary ($R_{\rm CM}$) to the surface ($R_{\rm s}$). Note that the relative speed $\boldsymbol{v}$ is the superposition of Earth's rotation and the speed of the low Earth orbit spacecraft, which is far beyond the velocities achievable in laboratory settings.[39]

For $V_{4+5}|_{\rm VV}$, $V_{4+5}|_{\rm AA}$, and V_{12+13}, the Earth must be modeled as a nucleon source. The expected potentials between the electrons and nucleons are as follows:

$$V_{\rm total} = \int_0^{2\pi}\int_0^{\pi}\int_0^{R_{\rm s}} r'^2 \sin\theta' \rho_{\rm n}(r') \times V(\boldsymbol{r}, \boldsymbol{v}, r', \theta', \varphi', r'_{\rm s}, \theta'_{\rm s}, \varphi'_{\rm s}) {\rm d}r' {\rm d}\theta' {\rm d}\varphi'. \quad (10)$$

The difference from Eq. (9) is that $\rho_{\rm n}(r')$ represents the density of Earth's unpolarized nucleons instead of that of polarized electrons. Additionally, the integration should cover the entire Earth from the center to the surface ($R_{\rm s}$).

Discussion. Because of the Yukawa-type $e^{-r/\lambda}$ factor, more geoelectrons and nucleons in the mantle contribute as λ increases. For λ well below the altitude of the low-Earth orbit spacecraft, that is, $\lambda \lesssim 100\,{\rm km}$, the improvements due to the high speed will be suppressed because the minimum r is the orbit altitude rather than approximately zero, as in the ground-based experiments.

In Ref. [37], using the measurements from two local Lorentz invariance (LLI) experiments,[42,64] the bounds on the coupling constants of different velocity-dependent spin–spin interactions between two electrons for various ranges of λ were obtained. In the current study, since we are only interested in improvements originating solely from the "Spacecraft-Earth" model itself, a meaningful comparison between the ground-based and space-based schemes should be conducted under the same sensitivity conditions. To this end, we assume an arbitrary energy sensitivity, e.g., $10^{-20}\,{\rm eV}$ for both the ground-based and space-based schemes to demonstrate the improvement from the "Spacecraft-Earth" model. Note that the energy sensitivity of the LLI experiment[42,64] has reached 10^{-21}–$10^{-22}\,{\rm eV}$ over the past decade. Today, significant progress has been made in detection techniques, and the sensitivity has improved by several orders of magnitude. We refer to Ref. [7] for a recent review. However, considering the challenges of the realistic, high-microgravity environment of a space experiment, we assumed such a sensitivity ($10^{-20}\,{\rm eV}$), which is slightly inferior to that of the LLI experiment, to conduct our simulations. It is clear that only the differences between ground-based and space-based experiments are meaningful, and applying a different sensitivity only shifts the absolute values of all couplings and thus does not alter the relative differences between schemes.

To demonstrate the periodicity of the signal expected in a space-based experiment, we assume that the China Space Station (CSS) is a likely experimental platform and consider the bounds in Ref. [37] for electron–electron (e–e) interactions between velocity-dependent spin–spin potentials as inputs to extract $V'_{\rm total}$ to be measured. We used $\lambda = 10^{2.5}\,{\rm km}$ (CSS orbital altitude) and $\lambda = 10^{5}\,{\rm km}$ (far exceeding the Earth's radius, where potentials saturate) as representative examples to present the results. The expected results for $\lambda = 10^{2.5}\,{\rm km}$ and $\lambda = 10^{5}\,{\rm km}$ are shown in Fig. 2, where the sensor is assumed to be heading east geographically during detection. In future experiments, such an oscillating potential can be obtained from the total pseudomagnetic field $\boldsymbol{B}_{\rm psd}$ measured by a magnetometer using $V = -\mu \cdot \boldsymbol{B}_{\rm psd}$, where μ is the magnetic moment of the sensor nucleus or electron. This is what was done in ground-based experiments, for example, Ref. [32].

These potentials exhibit clear periodicity as the CSS orbits Earth, which helps to extract signals from the background noise, thereby improving the accuracy of the experiment. Additionally, the line shapes of the various interactions differed significantly, suggesting that they could be distinguished in the space-based experiments. This provides unique opportunities to determine the magnitudes of the couplings and identify the types of interactions observed.

Once the spacecraft trajectory covers the entire area, a contour plot can be generated using the corresponding Two-Line Element (TLE) code such as the TLE for the CSS.[63] The most sensitive position for each interaction was determined. Because of the periodic orbital motion, signal-processing techniques can be applied to enhance the detection accuracy.

Again, we assume that the experiment is conducted on the CSS and use its TLE code,[63] as mentioned earlier, to generate the contour plot in Fig. 3. Because of the vector-based geographic relationships in the calculations, the potential measured at a given position may vary depending on the direction from which the CSS approaches. This implies that the potential detected when the CSS travels from south to north may differ from that detected when it travels from north to south. However, if the TLE data[63] remain unchanged, the contour plot remains fixed. Consequently, as the CSS orbits the Earth, the received signals exhibit periodic patterns for each orbit. Although slight differences in the signals may arise from variations in the angular velocity, the overall periodicity is sufficient for applying signal processing techniques to distinguish the signals from background noise, thereby improving the accuracy of the experiment.

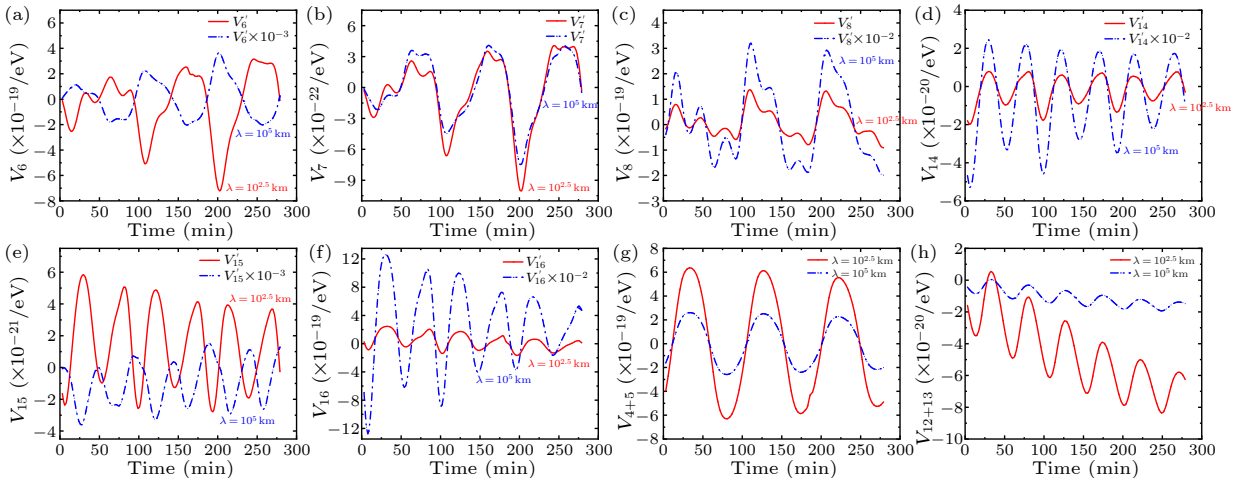

Fig. 2. Periodicity of the expected signals with the assumption that one can use the CSS as the spacecraft. The time axis starts on July 1, 2024.

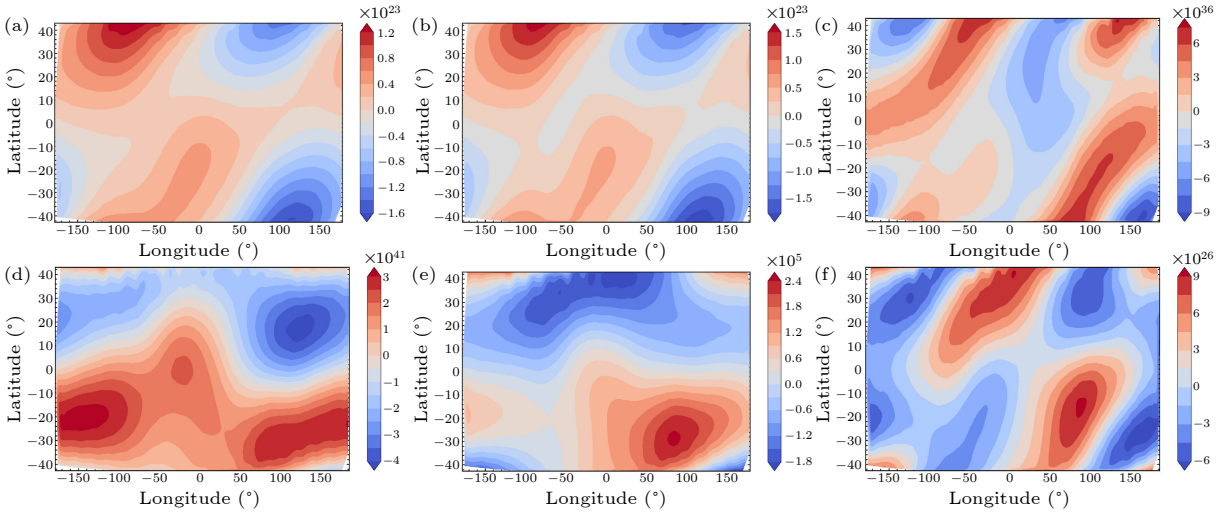

Fig. 3. Contour plots of the potentials expected as a spacecraft (CSS) travels from south to north. (a) V_6. (b) V_7. (c) V_8. (d) V_{14}. (e) V_{15}. (f) V_{16}.

In a previous study,[37,50] it was proposed that conducting experiments in southern Thailand would yield approximately twice the sensitivity compared to those performed in Amherst, owing to the stronger, more parallel surface magnetic field in Thailand. This highlights the importance of experimental location. In our study, the flexibility of the low-Earth orbit enabled it to cover different regions over time, enabling the identification of optimal locations for detecting new interactions at varying velocities. We believe that such an experiment will be highly effective in identifying the best areas to achieve the strongest signals, thereby significantly improving the sensitivity limits.

Compared with the works by Hunter *et al.*,[37,38,64] we found that the bounds on the electron (e) energy when its spin is oriented north (N) are generally less restrictive than when oriented east (E). This suggests that the most restrictive bounds are likely obtained through measurements in the eastward direction. Another key difference is that, unlike the experiments conducted on Earth, the potential of long-range interactions does not always maintain the same sign in space. As a spacecraft orbits the Earth, the angles between $\hat{\boldsymbol{\sigma}}_1$, $\hat{\boldsymbol{\sigma}}_2$, $\boldsymbol{r}$, and $\boldsymbol{v}$ change continuously. Consequently, it is natural to observe a potential oscillation between the positive and negative values, as illustrated in Fig. 2.

In Fig. 4, we present the expected upper bounds for all six exotic velocity-dependent spin–spin interaction couplings in e–e interactions as functions of the effective range λ, assuming an arbitrary energy resolution, for example, 10^{-20} eV, which does not affect the conclusions. Similar to the conclusion obtained in the ground-based experiment,[38] the coupling bounds of e–e interactions based on the new model with spin oriented north (N) are usually not as stringent as those with spin oriented east (E). The coupling constants for most of the interactions were expected to be constrained by at least three orders of magnitude. In less-sensitive regions, an improvement of at least one order of magnitude is feasible.

The bounds on the couplings of V_6 [Fig. 4(a)] and V_7 [Fig. 4(b)] are significantly lower. For V_6, at $\lambda = 10^{2.5}$ km, the new model results in a bound approximately 2.4 orders of magnitude more restrictive, and in the flatter regions, the improvement is at least 1.3 orders of magnitude. For V_7, the coupling bounds are reduced by approximately 1.6 orders of magnitude across the entire parameter range. Furthermore, the "Spacecraft-Earth" model enables the measurement of V_6 oriented east for λ less than 10^2 km, which is inaccessible to previous experiments.[38] Moreover, because V_{6+7} would be more meaningful than V_6 or V_7 individually for measurements,[7] we can further constrain V_{6+7} as

$$V_{6+7} = -\frac{\hbar}{4\pi c^2}\left(\frac{g_{\rm V}^1 g_{\rm A}^2}{2M_1} + \frac{g_{\rm A}^1 g_{\rm V}^2}{2M_2}\right) \times [(\hat{\boldsymbol{\sigma}}_1 \cdot \boldsymbol{v})(\hat{\boldsymbol{\sigma}}_2 \cdot \hat{\boldsymbol{r}})] \times \left(1 + \frac{r}{\lambda}\right)\frac{{\rm e}^{-r/\lambda}}{r^2}. \quad (11)$$

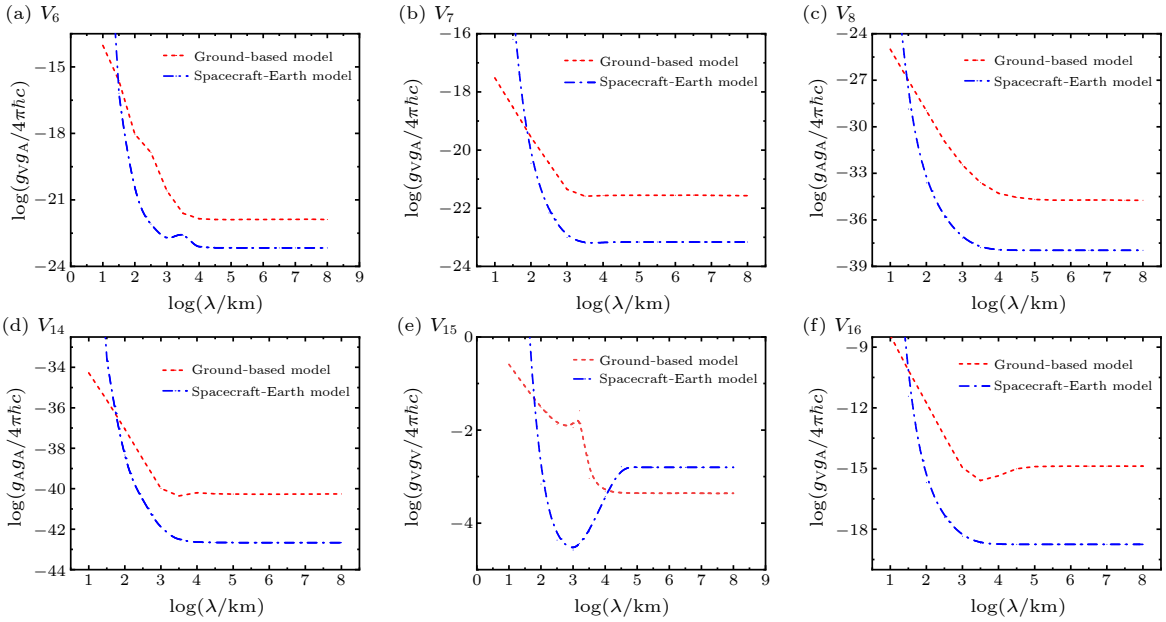

Fig. 4. Expected bounds on long-range spin–spin velocity-dependent couplings for electron–electron (e–e) interactions. The blue curves represent the expected constraints, assuming an arbitrary sensitivity condition, for example, 10^{-20} eV, where the result is the combination of the sensor assumed to be heading east (E) and north (N) during the detection. (a) Vector–axial (V–A) couplings [Eq. (1) with + sign] for V_6. (b) (V–A) coupling [Eq. (1) with − sign] for V_7. (c) (A–A) coupling [Eq. (2)] for V_8. (d) (A–A) couplings [Eq. (3)] for V_{14}. (e) (V–V) coupling [Eq. (4)] for V_{15}. (f) (V–A) coupling [Eq. (5)] for V_{16}.

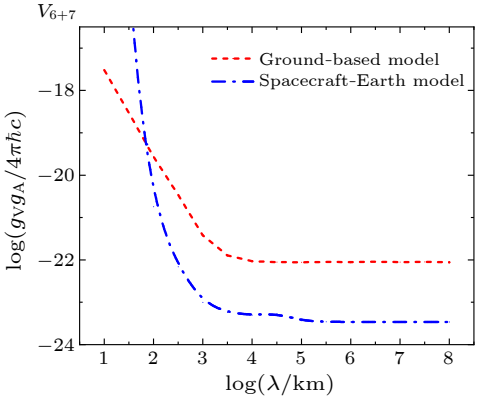

Fig. 5. Same as Fig. 4 but for V_{6+7}.

The bounds on the vector–axial (V–A) couplings of V_{6+7} (Fig. 5) are approximately 1.7 orders of magnitude more restrictive than those in the ground-based scheme for $\lambda = 10^{2.5}$ km, and at least 1.4 orders of magnitude more constrained in the flatter regions.

For $\lambda = 10^{2.5}$ km, the constraints on V_8, V_{14}, and V_{16} (Fig. 4) are improved by up to 5, 3, and 4 orders of magnitude, respectively, while in the flatter parameter regions, the constraints are tightened by approximately three orders of magnitude across all three interactions. However, one should note that the V_8 (V_{16}) constraints on the same coupling constant $g_A g_A$ ($g_V g_A$) are significantly weaker than those from V_{14} ($V_{6,7}$). The couplings for V_{15} [Fig. 4(e)] are approximately three orders of magnitude more restrictive for $\lambda = 10^{3.5}$ km compared with the ground-based scheme, whereas as λ increases, the improvement becomes less pronounced, indicating a more sensitive λ dependence. In Ref. [38], V_{15} is less reliable than other potentials, especially at short ranges, because it is more susceptible to local inhomogeneities. Our "Spacecraft-Earth" model can overcome this limitation and provide a more accurate constraint.

For long-range spin velocity-dependent electron–nucleon (e–N) interactions, the improvement mainly appears when λ exceeds the spacecraft altitude, as illustrated in Fig. 6. In particular, the improvement is approximately 1.5 orders of magnitude in the flatter areas and up to 2.5 orders of magnitude for $V_{4+5}|_{\mathrm{VV}}$ and $V_{4+5}|_{\mathrm{AA}}$ with $\lambda = 10^{2.5}$ km. In comparison, it is 2 orders of magnitude for the odd-parity spin velocity term V_{12+13}.

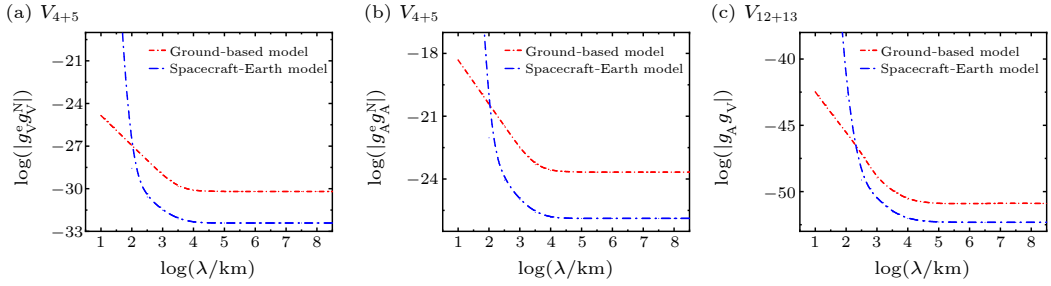

Fig. 6. Expected bounds on long-range spin–velocity-dependent couplings for electron–nucleon (e–N) interactions. The red and green curves represent the expected constraints, assuming an arbitrary energy-sensitivity condition, for example, 10^{-20} eV. (a) (V–V) coupling [Eq. (6)] for $V_{4+5}|_{\mathrm{VV}}$. (b) (A–A) coupling [Eq. (7)] for $V_{4+5}|_{\mathrm{AA}}$. (c) (A–V) coupling [Eq. (8)] for V_{12+13}.

Summary. In this paper, we propose a novel theoretical conjecture to further constrain the coupling constants of long-range velocity-dependent interactions, commonly referred to as the fifth force. Drawing on Earth as an enormous source, we propose that the high-velocity orbital operations of low-Earth-orbit spacecraft, whether satellites or space stations, can be exploited to overcome the limitations of ground-based experiments, such as fixed positions and slow speeds. The interaction strengths are simulated based on the periodic motion of the spacecraft. Because of the much higher relative velocity, the bounds on most of the six velocity-dependent spin–spin interactions are expected to be at least three orders of magnitude more restrictive than those in earlier measurements, whereas the two spin-velocity terms are at least 1.5 orders of magnitude more restrictive.

Previous studies[37,50] highlighted the significance of the experimental location. The flexibility of the spacecraft enables it to adapt over time, thereby optimizing the detection regions for the fifth force at varying velocities. The novel "Spacecraft-Earth" model identifies optimal regions for the strongest signals, significantly improving current limits. Unlike previous analyses, the unique periodic line shapes allow the distinction between different interaction contributions. Given the diversity of dark matter hypotheses, this approach helps identify plausible candidates and interaction types. Such periodicity also facilitates signal extraction from noise, thereby enhancing the experimental accuracy.

Although the proposed "Spacecraft-Earth" model has the potential to significantly improve the constraints on the coupling strength of spin-dependent interactions, conducting experiments in outer space remains a serious challenge. To achieve optimal sensitivity, it is necessary to address magnetic field shielding within the spacecraft, mitigate vibration-induced perturbations, and ensure the thermal stability of the environment in which the sensors operate. Consequently, the actual detection sensitivity of the sensor is likely lower than that on the ground. In addition, the inertial motion of the carrier should be considered, and a specific experimental scheme should be carefully designed in conjunction with the attitude of the spacecraft. However, significant advances in sensor sensitivity have been achieved, as reviewed in Ref. [7]. Thus, we are optimistic that the newly proposed "Spacecraft-Earth" model will significantly advance the detection of ultralight dark matter and tighten constraints on the exotic potentials discussed above.

Acknowledgements. This work was partially supported by the National Key R&D Program of China (Grant No. 2023YFA16067003) and the National Science Foundation of China (Grant Nos. 12435007 and 12522505).

References

[1] Bertone G, Hooper D, and Silk J 2005 *Phys. Rept.* **405** 279
[2] Frieman J, Turner M, and Huterer D 2008 *Ann. Rev. Astron. Astrophys.* **46** 385
[3] Peccei R D and Quinn H R 1977 *Phys. Rev. Lett.* **38** 1440
[4] Dine M and Kusenko A 2003 *Rev. Mod. Phys.* **76** 1
[5] Graham P W, Kaplan D E, and Rajendran S 2015 *Phys. Rev. Lett.* **115** 221801
[6] Safronova M S, Budker D, DeMille D, Kimball D F J, Derevianko A, and Clark C W 2018 *Rev. Mod. Phys.* **90** 025008
[7] Cong L, Ji W, Fadeev P *et al.* 2025 *Rev. Mod. Phys.* **97** 025005
[8] Moody J E and Wilczek F 1984 *Phys. Rev. D* **30** 130
[9] Dobrescu B A and Mocioiu I 2006 *J. High Energy Phys.* **11** 005
[10] Fadeev P, Stadnik Y V, Ficek F, Kozlov M G, Flambaum V V, and Budker D 2019 *Phys. Rev. A* **99** 022113
[11] Adelberger E G, Heckel B R, and Nelson A E 2003 *Ann. Rev. Nucl. Part. Sci.* **53** 77
[12] Wilczek F 1978 *Phys. Rev. Lett.* **40** 279
[13] Weinberg S 1978 *Phys. Rev. Lett.* **40** 223
[14] Jaeckel J and Ringwald A 2010 *Ann. Rev. Nucl. Part. Sci.* **60** 405
[15] An H, Pospelov M, Pradler J, and Ritz A 2015 *Phys. Lett. B* **747** 331
[16] Costantino A, Fichet S, and Tanedo P 2020 *J. High Energy Phys.* **03** 148
[17] Fichet S 2018 *Phys. Rev. Lett.* **120** 131801
[18] Barbosa S and Fichet S 2025 *J. High Energy Phys.* **01** 021
[19] Hammond G D, Speake C C, Trenkel C, and Pulido Paton A 2007 *Phys. Rev. Lett.* **98** 081101
[20] Heckel B R, Terrano W A, and Adelberger E G 2013 *Phys. Rev. Lett.* **111** 151802
[21] Terrano W A, Adelberger E G, Lee J G, and Heckel B R 2015 *Phys. Rev. Lett.* **115** 201801
[22] Ding J H, Wang J B, Zhou X *et al.* 2020 *Phys. Rev. Lett.* **124** 161801
[23] Chui T C P and Ni W T 1993 *Phys. Rev. Lett.* **71** 3247
[24] Long J C, Chan H W, Churnside A B, Gulbis E A, Varney M C M, and Price J C 2003 *Nature* **421** 922
[25] Ficek F, Kimball D F J, Kozlov M, Leefer N, Pustelny S, and Budker D 2017 *Phys. Rev. A* **95** 032505
[26] Ficek F, Fadeev P, Flambaum V V, Jackson Kimball D F, Kozlov M G, Stadnik Y V, and Budker D 2018 *Phys. Rev. Lett.* **120** 183002
[27] Vasilakis G, Brown J M, Kornack T W, and Romalis M V 2009 *Phys. Rev. Lett.* **103** 261801
[28] Crescini N, Carugno G, Falferi P, Ortolan A, Ruoso G, and Speake C C 2022 *Phys. Rev. D* **105** 022007
[29] Wu D, Liang H, Jiao M, Cai Y F, Duan C K, Wang Y, Rong X, and Du J 2023 *Phys. Rev. Lett.* **131** 071801
[30] Liang H, Jiao M, Huang Y, Yu P, Ye X, Wang Y, Xie Y, Cai Y F, Rong X, and Du J 2023 *Natl. Sci. Rev.* **10** nwac262
[31] Zhang S, Ba Z, Ning D, Zhai N, Lu Z, and Sheng D 2023 *Phys. Rev. Lett.* **130** 201401
[32] Wei K, Ji W, Fu C, Wickenbrock A, Fang J, Flambaum V V, and Budker D 2022 *Nat. Commun.* **13** 7387
[33] Kotler S, Ozeri R, and Kimball D F J 2015 *Phys. Rev. Lett.* **115** 081801
[34] Rong X, Wang M Q, Geng J P *et al.* 2018 *Nat. Commun.* **9** 739
[35] Rong X, Jiao M, Geng J, Zhang B, Xie T, Shi F, Duan C K, Cai Y F, and Du J 2018 *Phys. Rev. Lett.* **121** 080402
[36] Yan H, Sun G A, Peng S M, Zhang Y, Fu C B, Guo H, and Liu B Q 2015 *Phys. Rev. Lett.* **115** 182001
[37] Hunter L, Gordon J, Peck S *et al.* 2013 *Science* **339** 928
[38] Hunter L R and Ang D G 2014 *Phys. Rev. Lett.* **112** 091803
[39] Clayburn N B and Hunter L R 2023 *Phys. Rev. D* **108** L051701
[40] Venema B J, Majumder P K, Lamoreaux S K, Heckel B R, and Fortson E N 1992 *Phys. Rev. Lett.* **68** 135
[41] Jackson Kimball D F, Dudley J, Li Y, Patel D, and Valdez J 2017 *Phys. Rev. D* **96** 075004 [Erratum: 2023 *Phys. Rev. D* **107** 019903]
[42] Heckel B R, Adelberger E G, Cramer C E *et al.* 2008 *Phys. Rev. D* **78** 092006
[43] Wu L Y, Zhang K Y, Peng M, Gong J, and Yan H 2023 *Phys. Rev. Lett.* **131** 091002
[44] Leefer N, Gerhardus A, Budker D, Flambaum V V, and Stadnik Y V 2016 *Phys. Rev. Lett.* **117** 271601
[45] Tsai Y D, Farnocchia D, Micheli M, Vagnozzi S, and Visinelli L 2024 *Commun. Phys.* **7** 311

[46] Wineland D J, Bollinger J J, Heinzen D J, Itano W M, and Raizen M G 1991 *Phys. Rev. Lett.* **67** 1735
[47] Youdin A N, Krause D, Jagannathan K, Hunter L R, and Lamoreaux S K 1996 *Phys. Rev. Lett.* **77** 2170
[48] Ni W T, Pan S S, Yeh H C, Hou L S, and Wan J L 1999 *Phys. Rev. Lett.* **82** 2439
[49] Huang X M, Wang Y H, Kang X *et al.* 2025 *Phys. Rev. D* **112** 095015 (arXiv:2410.15755 [quant-ph])
[50] Tian Y and Zhao D 2012 *Phys. Earth Planet. Inter.* **200** 72
[51] Dobrescu B A 2005 *Phys. Rev. Lett.* **94** 151802
[52] Chu P H, Ristoff N, Smits J, Jackson N, Kim Y J, Savukov I, and Acosta V M 2022 *Phys. Rev. Res.* **4** 023162
[53] Dziewonski A M and Anderson D L 1981 *Phys. Earth Planet. Inter.* **25** 297
[54] Irifune T, Shinmei T, McCammon C A, Miyajima N, Rubie D C, and Frost D J 2010 *Science* **327** 193
[55] Jeanloz R, Knittle E, O'Nions R K, Clayton R, and Parsons B 1989 *Philos. Trans. R. Soc. Lond. A* **328** 377
[56] Morgan J W and Anders E 1980 *Proc. Natl. Acad. Sci. U.S.A.* **77** 6973
[57] Wang H S, Lineweaver C H, and Ireland T R 2018 *Icarus* **299** 460
[58] Buffett B and Davis W 2018 *Geophys. Res. Lett.* **45** 1845
[59] Stacey F D 1977 *Phys. Earth Planet. Inter.* **15** 341
[60] Chulliat A, Brown W, Alken P *et al.* 2020 *The USUK World Magnetic Model for 2020–2025: Technical Report*
[61] Buffett B A, Garnero E J, and Jeanloz R 2000 *Science* **290** 1338
[62] Rhodes B *Skyfield: High precision research-grade positions for planets and earth satellites* [Computer software]
[63] China Manned Space Agency 2024 *China Manned Space Official Website* [Online]
[64] Peck S K, Kim D K, Stein D, Orbaker D, Foss A, Hummon M T, and Hunter L R 2012 *Phys. Rev. A* **86** 012109